Precision evaluation of nitrogen isotope ratios by Raman spectrometry

Yamamoto, Junji
Department of Earth and Planetary Sciences, Graduate School of Science Kyushu University

Hagiwara, Yuuki
Graduate School of Science Hokkaido University

出版情報：Analytical Science Advances. 3 (9-10), pp.269-277, 2022-10-17. Wiley
バージョン：

Research Article
doi.org/10.1002/ansa.202200020

Chemistry Europe
European Chemical Societies Publishing

Received: 3 June 2022

Revised: 12 August 2022

Accepted: 17 August 2022

Precision evaluation of nitrogen isotope ratios by Raman spectrometry

Junji Yamamoto[1] | **Yuuki Hagiwara**[2,3]

[1]Department of Earth and Planetary Sciences, Graduate School of Science, Kyushu University, Nishi-ku, Japan

[2]Graduate School of Science, Hokkaido University, Kita-ku, Japan

[3]Research Institute for Marine Geodynamics, Japan Agency for Marine–Earth Science and Technology, Yokosuka, Japan

Correspondence
Junji Yamamoto, Department of Earth and Planetary Sciences, Graduate School of Science, Kyushu University, 744 Motooka, Nishi-ku, Fukuoka 819-0395, Japan.
Email: yamamoto@geo.kyushu-u.ac.jp

Funding information
Japan Society for the Promotion of Science, Grant/Award Numbers: 20H02000, 20K20931

Abstract

We measured Raman spectra of N_2 fluids obtained at 0.1–25 MPa at room temperature. The $^{14}N^{15}N$ peak in the Raman spectrum of a low-pressure N_2 fluid is difficult to detect because of the prevalence of a group of peaks attributed to rotational vibration of $^{14}N_2$. The Raman peaks of $^{14}N^{15}N$ and $^{14}N_2$ of N_2 fluid at 25 MPa were acquired at various exposure times. The mean values and standard deviations of the peak height ratios and peak area ones of $^{14}N^{15}N$ and $^{14}N_2$ were examined for each time. The standard deviations of the peak height ratios and peak area ones were 2.2% and 1.9%, respectively, for 20 spectra acquired with peak height of 1 million counts of $^{14}N_2$. The uncertainties are about two times higher than those predicted from the noise of a CCD. Improvement of the pixel resolution can enhance the precision of the nitrogen isotope ratios by Raman spectroscopy.

KEYWORDS
error, high-pressure, isotope ratio, optical cell, Raman spectroscopy

1 | INTRODUCTION

Minerals occasionally contain fluids, called fluid inclusions. By measuring the isotope ratios of gases extracted by crushing minerals in vacuum, the origin of the fluid and the formation process of the host minerals have been discussed. Fluid inclusions of several types are commonly found, each of which could have a different origin. Discussion of the Earth's material cycle system using fluid inclusions necessitates analyses of the isotopic ratios of individual fluid inclusions. For this purpose, micro-Raman spectroscopy has been applied to estimate the carbon isotope ratio of CO_2, the main component of fluid inclusions in the Earth's deep interior.[1,2] Arakawa et al.[3] reported that carbon isotope ratios of CO_2 can be ascertained with precision of 20‰ using Raman spectrometry. Yokokura et al.[4] improved the precision to 8.7‰. Application of the method to natural fluid inclusions is imminent because the variation in the carbon isotope ratio of natural carbon dioxide is about 30‰.

Nevertheless, constraining the origin of carbon in the Earth's interior solely on the basis of carbon isotope ratios is difficult. In fact, there are three or more possible origins of carbon circulating in the Earth's interior: primordial carbon in mantle, carbonate soils, and coral reefs subducted into the Earth's interior with oceanic plates.[5] To evaluate the contribution of the end-members for carbon, other indices are needed.

Although water is the major known component of fluid inclusions found in minerals in the Earth's deep interior,[6,7] the isotopic ratios of hydrogen and oxygen of materials in the Earth's interior are not well constrained. The third major component in fluid inclusions of minerals in the Earth's interior is N_2.[8–11] Isotopic ratios of nitrogen and noble gases extracted by crushing mantle minerals in vacuum have been used to discuss the origins of fluids in fluid inclusions.[12,13] Analysis of nitrogen isotope ratios of N_2 in the fluid inclusions using micro-Raman spectroscopy is expected to improve the discussion of the origin of the fluid. Raman spectra of N_2 fluids have been reported in many

Research Article
doi.org/10.1002/ansa.202200020
Chemistry Europe
European Chemical Societies Publishing

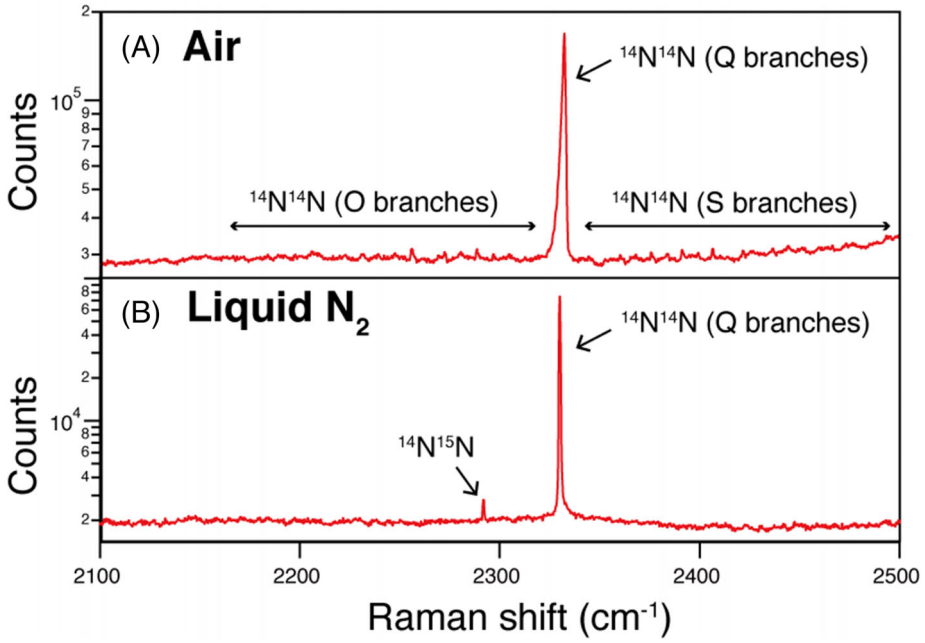

FIGURE 1 Raman spectrum of (A) N_2 (0.1 MPa lab air, 3 h exposure) and (B) liquid N_2 (liquid nitrogen poured into a petri dish under room temperature (~20°C) and pressure, 1 min exposure)

works.[14–16] Some of them include detections of $^{14}N_2$($^{14}N^{14}N$) as well as $^{14}N^{15}N$ and $^{15}N_2$($^{15}N^{15}N$).[17–20] Nevertheless, no report of the relevant literature has specifically described the nitrogen isotope ratio with error. For this study, we evaluate the precision of $^{14}N^{15}N/^{14}N_2$ of N_2 fluid using micro-Raman spectroscopic analysis, with a view to natural applications. Materials derived from Earth's interior such as volcanic rocks, fumarolic gases, and peridotites show $\delta^{15}N$ (‰), which is defined as $[\{(^{15}N/^{14}N)_{sample} - (^{15}N/^{14}N)_{air}\}/(^{15}N/^{14}N)_{air}] \times 1000$, ranging from −20% to 10‰.[12,13] Therefore, as a first step, the target precision for this method is below ± 15‰.

2 | SAMPLES AND EQUIPMENTS

2.1 | N_2 fluid

Figure 1A shows the Raman spectrum of air obtained at 0.1 MPa and room temperature. The Q branches of $^{14}N_2$ and groups of peaks of O and S branches of $^{14}N_2$ can be recognized. Some O branches of $^{14}N_2$ overlap with the Q branches of $^{14}N^{15}N$ at around 2291 cm^{-1}, making it difficult to measure $^{14}N^{15}N/^{14}N_2$ of N_2 in air using Raman spectroscopy. Kim et al.[19] proposed polarization lock-in filtering (PLF) as a technique to decrease the O and S branches of $^{14}N_2$. Actually, PLF technique is a filtering method that is capable of suppressing polarization-independent signals such as blackbody radiation and most fluorescence. Using the technique, they obtained $^{14}N^{15}N/^{14}N_2 = 0.7\%$ for air using Raman spectroscopy, with results showing good agreement with the known natural abundance of $^{14}N^{15}N$ (0.73% in the ambient air). As an alternative, some potential exists in using high-density N_2 fluid for the identification of $^{14}N^{15}N/^{14}N_2$ by Raman spectroscopy. Figure 1B shows the Raman spectrum of liquid nitrogen (−196°C). The O and S branches of $^{14}N_2$ are small. Therefore, the Q branches of $^{14}N^{15}N$ are clearly visible. However, liquid nitrogen in open systems changes the nitrogen isotope ratio through boiling and evaporation. To prevent isotopic fractionation, the system must be kept closed by sealing it in a cooling device or in a pressure-resistant container. For this study, we applied a high-pressure N_2 fluid encapsulated in a pressure-resistant optical cell.

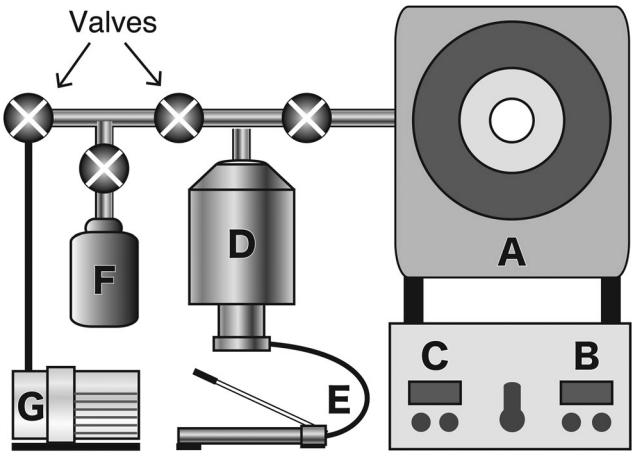

FIGURE 2 High-pressure optical cell and an apparatus for making high-pressure N_2 fluid: (A) optical cell; (B) pressure gauge; (C) thermometer; (D) pressurizer; (E) hydraulic pump; (F) liquid N_2 cylinder; (G) rotary pump

Figure 2 portrays the apparatus used for producing high-pressure N_2 fluid. First, the apparatus was evacuated with a rotary pump; then a cylinder was filled with liquid nitrogen made by cooling purified air.

Research Article
doi.org/10.1002/ansa.202200020
Chemistry Europe
European Chemical Societies Publishing

As the temperature rises, the liquid nitrogen transforms into supercritical N_2 fluid, which fills the apparatus. Subsequently, by reducing the volume of the line with a pressurizer, N_2 fluid of up to 25 MPa can be prepared in an optical cell. The optical cell is equipped with a sapphire window to obtain Raman signals of the high-pressure N_2 fluid. Pressure in the optical cell can be controlled by the pressurizer. The pressure and temperature of N_2 fluid during the present analyses were, respectively, 0–25 MPa and 20.1–20.8°C.

2.2 | Micro-Raman spectroscopy

Raman spectra were acquired using diode-pumped solid-state laser (532 nm, Gem 532; Laser Quantum) excitation, a spectrometer with 75 cm focal length (Acton SP-2750; Princeton Instruments, Inc.), and a CCD camera (1650 × 200 pixels, 16 μm width, iVac; Andor Technology). The laser was focused through a 10× objective (N.A. = 0.2, T Plan SLWD; Nikon Corp.). The laser output was 1 W at the source and approximately 0.4 W at the surface of the sapphire window. The pixel resolution of the present Raman system when using a grating of 1800 lines/mm is 0.25 cm^{-1}/pixel at around 2300 cm^{-1}. Spectra were collected in a single window between 2091 and 2501 cm^{-1}, which covers the Q branches of $^{14}N_2$ at around 2330 cm^{-1} and those of $^{14}N^{15}N$ at around 2291 cm^{-1}. Each band of $^{14}N_2$ and $^{14}N^{15}N$ was fitted to a split pseudo-Voigt curve by using "Fityk software."[21] The curve-fitting served to improve accuracy of peak heights and areas. The wavenumber was corrected using neon lines.

3 | ANALYTICAL CONDITIONS

3.1 | Pressure of N_2 fluid

To evaluate the effectiveness of pressure for reducing the O branches of $^{14}N_2$, we prepared N_2 fluids with six pressures at 5 MPa intervals from 0 to 25 MPa and measured their Raman spectra (Figure 3). The spectrum at 0 MPa (Figure 3A) was obtained from the cell under vacuum. Nevertheless, a $^{14}N_2$ peak was observed at 2330 cm^{-1}, which would be a signal derived from N_2 in the air outside the cell. In Figure 3, the increase in intensity over the entire wavenumber range with exposure time results from the fluorescence generated from the sapphire window of the cell. At 5 MPa, the influence of O branches on the $^{14}N^{15}N$ peak at 2291 cm^{-1} is not small (upper left box in Figure 3B). Although the influence is also recognized at 10 and 15 MPa, it is not apparent at 20 MPa. To eliminate the influence of O branches in the analysis of $^{14}N^{15}N/^{14}N_2$ of N_2 fluid, it is necessary to apply N_2 fluid at pressure of 20 MPa or higher at room temperature. It is noteworthy that with increasing pressure, the tail of the $^{14}N_2$ peak broadens and approaches the $^{14}N^{15}N$ peak. Both peaks are separated clearly in the pressure range up to 25 MPa. Therefore, we investigate the precision of the $^{14}N^{15}N/^{14}N_2$ using 25 MPa N_2 fluid, which has the influence of neither O branches nor the broadening of $^{14}N_2$ peak on $^{14}N^{15}N$ peak (Figure 3F).

TABLE 1 Calculated uncertainties (%) of $^{14}N^{15}N/^{14}N_2$ caused by noises of a CCD

Intensity	σ_S	σ_D	σ_R	Total noises	Time (s)*
1000	24.04	0.39	65.21	69.50	2
10,000	7.61	0.13	6.53	10.02	17
100,000	2.41	0.04	0.65	2.49	167
1,000,000	0.76	0.01	0.22	0.79	1667

*Duration to obtain each intensity assuming intensity rate of $^{14}N_2$ is ~600 count/s.

3.2 | Exposure time

To ascertain the exposure time, we calculated the uncertainty of $^{14}N^{15}N/^{14}N_2$ attributable to various noises of the CCD used. The equation for the noise of a CCD is expressed as

$$\sqrt{{\sigma_S}^2 + {\sigma_D}^2 + {\sigma_R}^2},$$

where σ_S, σ_D, and σ_R respectively represent the shot noise, the dark noise, and readout noise. σ_S is the square root of the signal counts of a peak. σ_D is designated as the dark current arising from thermal energy in the silicon structure of a CCD. σ_R is defined as the noise in the amplifier on the CCD chip, which converts the stored charge of each pixel into an analog voltage. The values of σ_D and the σ_R were obtained from blank measurements of the spectrometer at various exposure times and numbers of accumulation.

The estimation results of the noises are presented in Table 1. The intensity in Table 1 represents approximate peak height of $^{14}N_2$ peak. The σ_D does not contribute to the total noises in any intensity region. In the 10^3-count region, the contribution of σ_R is large, but in the 10^4-count region, the influence of σ_S and σ_R is comparable. In the higher intensity region, the total error is represented by σ_S. All the noise is negatively correlated with intensity and is expected to result in all errors at approximately permil-order in the million-count range and above. It takes about half an hour to obtain 10^6 counts of $^{14}N_2$ peak from 25 MPa N_2 fluid with the present spectrometer. It is not practical to apply exposure times longer than that described above because the effects of other factors, such as deformation of a spectrometer with room temperature change, will appear during measurements.

4 | RESULTS AND DISCUSSION

4.1 | Peak height ratios and peak area ones of N_2 Raman peaks

We measured Raman spectra of 25 MPa N_2 fluid 20 times in each of four intensity regions of 10^3, 10^4, 10^5, and 10^6 counts. Figure 4 presents the measured data. The $^{14}N^{15}N/^{14}N_2$ peak height ratios (H_{29}/H_{28}) and peak area ratios (A_{29}/A_{28}) for each intensity region and their standard deviations are presented in Table 2. We note here that we also include the H_{29}/H_{28} to investigate the precision of

Research Article
doi.org/10.1002/ansa.202200020
Chemistry Europe
European Chemical Societies Publishing

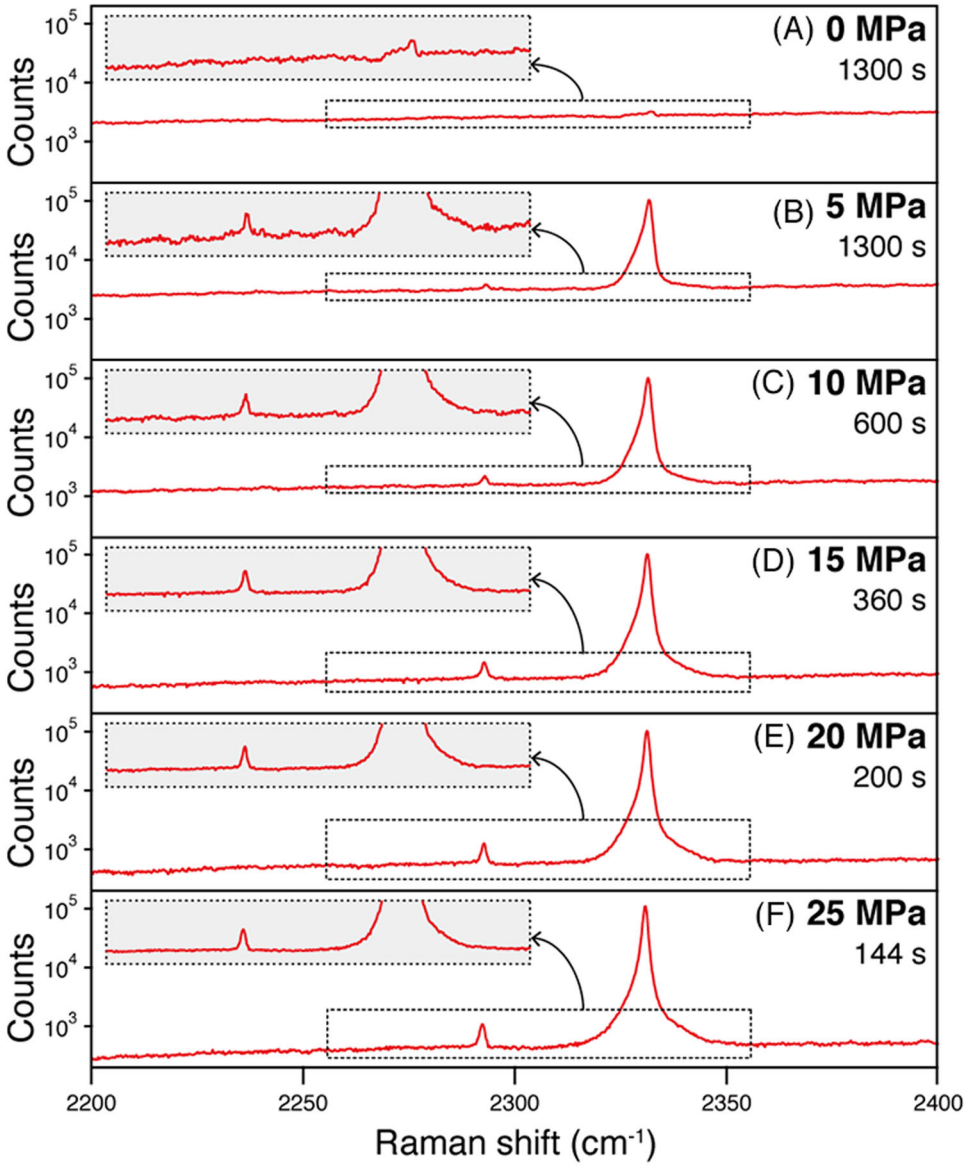

FIGURE 3 Raman spectra of N_2 fluid at various pressures in a high-pressure optical cell. The pressures of the N_2 fluid are presented in the upper right corner of (A–F). The numbers of seconds below them are exposure times. In (B–F), the exposure time was adjusted to achieve intensity of about 10^5 counts of $^{14}N_2$. The exposure time in (A) is the same as the time at 5 MPa (B). Boxes in the upper left corner of the respective graphs are enlarged graphs with linear vertical axes.

TABLE 2 Peak height ratios and peak area ones of $^{14}N^{15}N$ and $^{14}N_2$ Raman peaks in four intensity regions

Intensity region	H_{29} / H_{28}	1σ	1σ (%)	A_{29} / A_{28}	1σ	1σ (%)
1000	0.010105	0.003104	30.72	0.009773	0.002933	30.01
10,000	0.007190	0.000535	7.44	0.006899	0.000643	9.33
100,000	0.006218	0.000199	3.19	0.006093	0.000336	5.51
1,000,000	0.006400	0.000139	2.17	0.006486	0.000123	1.90

Note: Data were obtained from 20 measurements of N_2 fluid at 25 MPa at room temperature. The intensities of the 20 data in each intensity region have variation of less than 5%.

Research Article
doi.org/10.1002/ansa.202200020
Chemistry Europe
European Chemical Societies Publishing

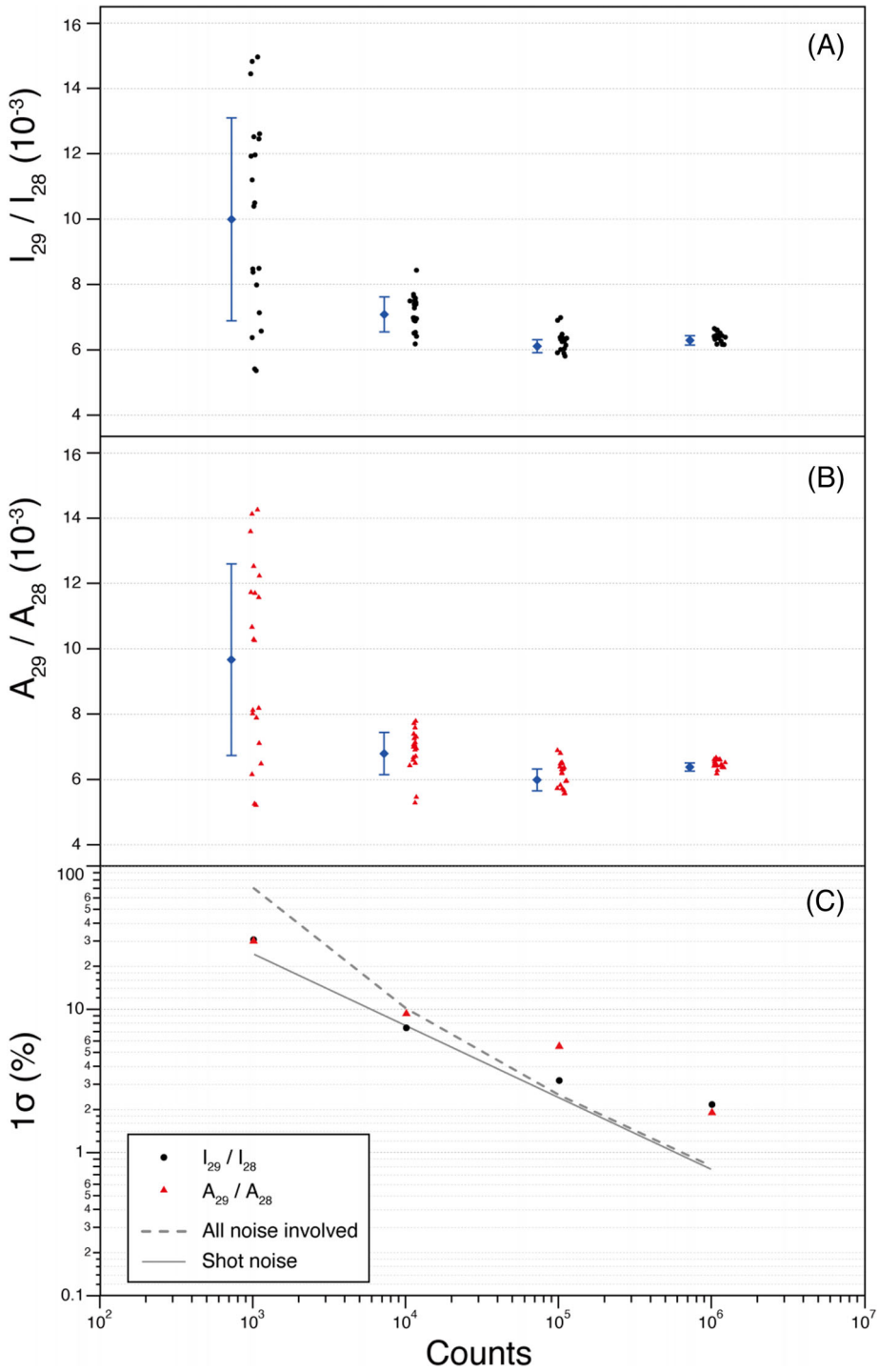

FIGURE 4 Number of counts of $^{14}N_2$ Raman peaks of 25 MPa N_2 fluid versus peak height ratios (H_{29}/H_{28}) (A) and peak area ratios (A_{29}/A_{28}) (B) of $^{14}N^{15}N$ and $^{14}N_2$ Raman peaks, and their standard deviations (C). Data with error bars in (A) and (B) are the mean and standard deviation of 20 peak height ratios and peak area ones for each of the four intensity regions.

$^{14}N^{15}N/^{14}N_2$. This is because A_{29}/A_{28} might be influenced by possible composites of other small peaks.

The uncertainty in both H_{29}/H_{28} and A_{29}/A_{28} decreased with intensity, yielding uncertainties of 2.2% and 1.9%, respectively, at 10^6 counts. These values do not achieve the target precision of 1.5% required to apply the method to natural materials. Considering their error ranges, the H_{29}/H_{28} and A_{29}/A_{28} mutually overlap in the intensity regions of 10^5 and 10^6 counts.

It is noteworthy that the H_{29}/H_{28} and A_{29}/A_{28} in the 10^3-count regions do not overlap with the10^5- and 10^6-count values (Table 2). If the H_{29}/H_{28} and A_{29}/A_{28} change with intensity, then it would be a severe problem for determining the nitrogen isotope ratios using

Research Article
doi.org/10.1002/ansa.202200020
Chemistry Europe
European Chemical Societies Publishing

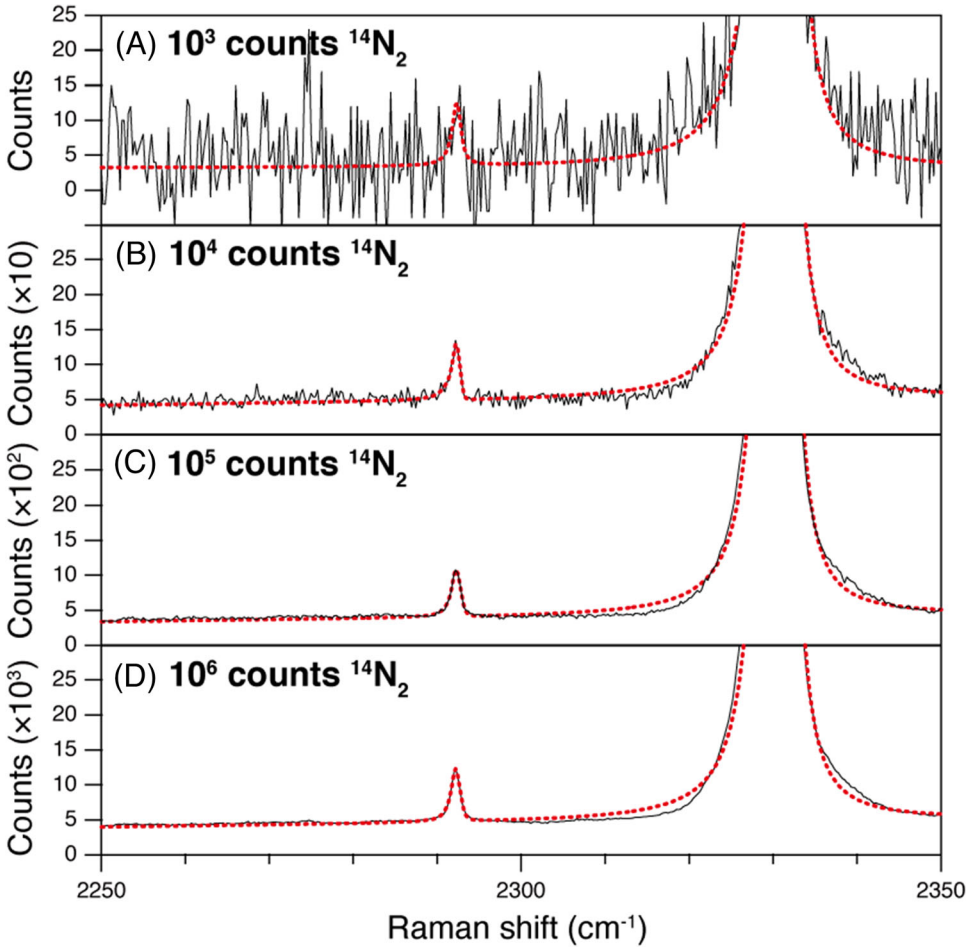

FIGURE 5 Raman spectra of N_2 fluid at 25 MPa, showing the $^{14}N^{15}N$ peak and the root of the $^{14}N_2$ peak. (A), (B), (C), and (D) respectively portray the spectra at the counts of $^{14}N_2$ of approximately 10^3, 10^4, 10^5, and 10^6. The dashed lines are the results of curve-fitting.

Raman spectroscopy. In the 10^3-count region, although the data for both ratios varied widely, the H_{29}/H_{28} and A_{29}/A_{28} were noticeably higher than the values in the high intensity regions (Figure 4). Actually, a paired *t*-test for the data between 10^3- and 10^4-count regions indicates significant difference for H_{29}/H_{28} ($p = 0.0005$) and for A_{29}/A_{28} ($p = 0.0006$). As a factor affecting the H_{29}/H_{28} and A_{29}/A_{28}, we investigate the effect of spectral noise on the peak shape.

Figure 5 shows spectra in the four intensity regions. To make it easier to evaluate the effects of noise on the $^{14}N^{15}N$ peaks at around 2291 cm^{-1}, we specifically examined the approximately 2.5% region of the peak height of $^{14}N_2$ peaks. The $^{14}N^{15}N$ peak in the 10^3-count region is not easy to distinguish from noise. The high H_{29}/H_{28} and A_{29}/A_{28} in the 10^3-count regions might be attributable to the discrimination threshold between the tail of the $^{14}N^{15}N$ peak and noise, which were intermingled with each other in the curve-fitting process. In the intensity region of 10^4 counts or more, where the effect of noise on the peak shape becomes small, no difference in H_{29}/H_{28} or A_{29}/A_{28} is visible among the intensity regions. We can obtain reliable H_{29}/H_{28} and A_{29}/A_{28} if there is sufficient intensity to ignore noise effects on the peak shape.

Interestingly, even for peak areas that directly reflect Raman intensity, A_{29}/A_{28} differs from the atmospheric value (0.0073) beyond the error range. Although accuracy of isotopic ratios is not the main topic of this study, we briefly consider the possibility contributing to the difference. A possible reason is that the peak shapes differ between $^{14}N_2$ and $^{14}N^{15}N$. Figures 3 and 5 show that the $^{14}N_2$ peak is asymmetric. This is true because it is an aggregate of Q branches, which are derived at rotational quantum numbers greater than 1.[17,22,23] Although the $^{14}N^{15}N$ peak is also asymmetric,[18] its asymmetry is seemingly different from that of the $^{14}N_2$ peak (Figures 3 and 5). The difference in asymmetry between both peaks affects the fitting degree. If it is the reason for the difference from the air value, then it would not present any difficulty in the determination of the nitrogen isotope ratios because this discrepancy can be corrected using a standard N_2 fluid with a known isotopic ratio.

4.2 | Precision of H_{29}/H_{28} and A_{29}/A_{28}

Considering the ~30‰ variation range in nitrogen isotope ratios of natural materials, with the precision of 2.2% for the peak height

Research Article
doi.org/10.1002/ansa.202200020
Chemistry Europe
European Chemical Societies Publishing

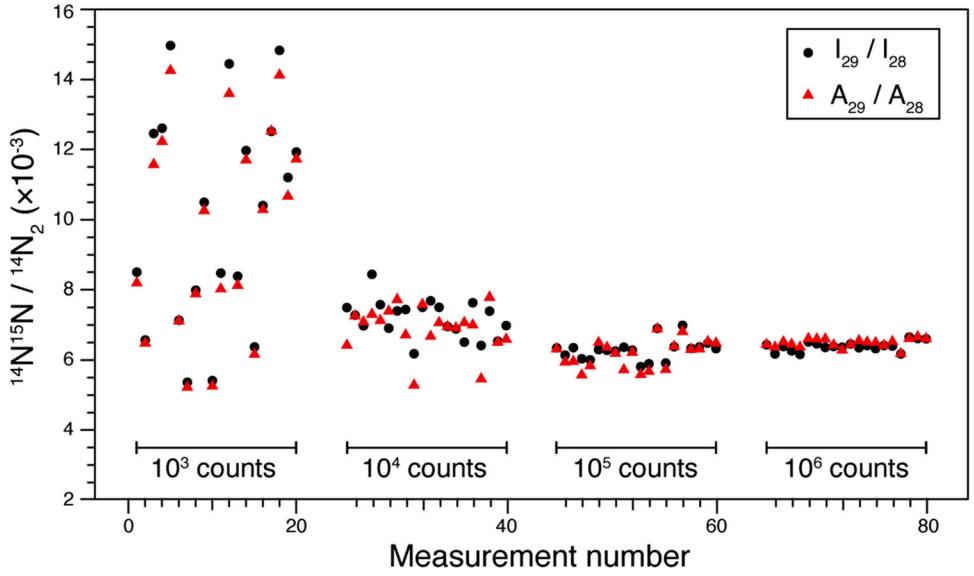

FIGURE 6 Relation between the order of analysis of H_{29}/H_{28} and A_{29}/A_{28}

ratio and 1.9% for the peak area ratio, it is difficult to apply this method to natural materials. We discuss here what contributes to the improvement of precision.

The order of magnitude of the uncertainty and the fact that the uncertainties decrease with intensity for both ratios are consistent with the calculation of CCD noises, but the deviation between the two approaches increases concomitantly with increasing intensity (Tables 1 and 2, Figure 4C). Figure 4C shows the uncertainties of both approaches and suggests that the uncertainties in the region below 10^4 counts are explainable by the CCD noises. Although we expected from the noise calculations that nitrogen isotope ratios in the 10^6-count region can be determined with uncertainty of approximately a permil (see section "exposure time"), it is more than twice, which indicates that there is another factor, aside from the CCD noise, responsible for the uncertainty, especially with the analytical conditions for which high intensities were obtained.

Long analysis duration to obtain high intensities increases the likelihood that the data are affected by changes in alignment. Figure 6 shows the data in the order of measurements. In the 10^5-count and 10^6-count regions, there would be both gradual and abrupt changes in the data, indicating the existence of a factor other than randomly generated noise. That change might be a reason for the measurement uncertainty, which is greater than the calculated CCD noises, especially in the 10^6-count region. The following are possible factors that can alter the height or area of Raman peaks during measurements: changes in laser power and the temperature of samples or a spectrometer, and shifts in specific examination of the sample.[24] They are expected to have similar effects both on $^{14}N^{15}N$ and $^{14}N_2$. In other words, they do not affect the H_{29}/H_{28} and A_{29}/A_{28}. In contrast, fluctuations in the wavenumber of the Raman peaks might have an indirect influence on both ratios. Arakawa et al.[3] proposed the possibility that the height of a Raman peak changes with the position where it hits the CCD. The pixel resolution of the equipment used for this study is 0.25 cm^{-1}/pixel at 2300 cm^{-1}, which is much better than that of Arakawa et al.[3] (approx. 1.2 cm^{-1}/pixel at 2300 cm^{-1}). However, because the width at half maximum of the N_2 peaks is about 1.3 cm^{-1}, only six pixels are used to detect the peak fragments with peak height higher than half of the maximum height of the peak. Wavenumber fluctuations might change the relative positions of the peaks to the CCD, leading to changes in the shape of the detected peaks and possibly changing the H_{29}/H_{28} and A_{29}/A_{28}.

Various possible causes of wavenumber fluctuations exist, such as physical shocks or vibrations to a spectrometer, deformation of the spectrometer by changes in room temperature, and changes in the sample state.[25,26] We examined fluctuations in the wavenumber and height of the N_2 peaks during the approximately 9 h of measurements taken in the 10^6-count region. Figure A1 shows variation of the H_{29}/H_{28}, A_{29}/A_{28}, intensity, and wavenumber of the N_2 peaks among measurements taken in the 10^6-count region. Both $^{14}N^{15}N$ and $^{14}N_2$ peaks have about 20% variation in intensity. Their wavenumbers fluctuate highly initially and converge gradually to lower values over time. The wavenumber fluctuation during the measurement is about 0.06 cm^{-1} for both peaks. Considering the pixel resolution of the present equipment (0.25 cm^{-1}/pixel), it is possible that the wavenumber fluctuation changes the positional relation between the peaks and pixel configuration, resulting in changes in the detected peak shapes, that is, changes in peak height and peak area. Although the influence affects both $^{14}N^{15}N$ and $^{14}N_2$ peaks, the directions of change in their height and area might not be identical, engendering variation in both H_{29}/H_{28} and A_{29}/A_{28}. The description presented above is only one interpretation of the fact that the measurement uncertainty is greater than the calculated value. If that is correct, then the diminishing wavenumber fluctuation is fundamentally important to improve the precision of isotopic analyses by Raman spectroscopy. For this purpose, reducing temperature fluctuation and exposure time might be effective. In addition, the better pixel resolution contributes to more precise peak shapes, improving the precision of isotope ratios.

Research Article
doi.org/10.1002/ansa.202200020

Finally, we note an important point for the application of the method to natural N_2-bearing fluid inclusions. Most of the N_2-bearing fluid inclusions reported are mixtures with CO_2 having various pressure.[8–11] In order to determine the nitrogen isotope ratios of such fluid inclusions, it is necessary to investigate the dependence of the N_2 Raman peak area on chemical composition and pressure.

5 | SUMMARY

Using high-pressure N_2 fluid, we reduced the Raman peaks of N_2 originating from the rotational vibration, thereby enabling the measurement of $^{14}N^{15}N/^{14}N_2$ using Raman spectroscopy. The H_{29}/H_{28} and A_{29}/A_{28} of the measured $^{14}N^{15}N$ and $^{14}N_2$ Raman peaks for 25 MPa N_2 fluid were, respectively, 0.006400 ± 0.000139 (2.2%) and 0.006486 ± 0.000123 (1.9%) in the intensity region of one million counts of $^{14}N_2$. Although the calculation of the uncertainty induced by the noise of a CCD demonstrated the potential to ascertain $^{14}N^{15}N/^{14}N_2$ to less than 1% at about one million counts of $^{14}N_2$, the measurement uncertainties are about twice as high as those of the calculated values. This uncertainty might be attributable to the change in the fitting shape of the Raman peaks caused by fluctuation of the wavenumber during the measurements. Applying a spectrometer with higher pixel resolution would allow the determination of nitrogen isotope ratios with permil-order uncertainty.

ACKNOWLEDGEMENTS

This study was supported by Grants-in-Aid for Scientific Research (grant numbers: 20H02000 and 20K20931) from the Japan Society for the Promotion of Science.

CONFLICT OF INTEREST

The authors declare no conflict of interest.

DATA AVAILABILITY STATEMENT

Data available upon request.

REFERENCES

1. Yamamoto J, Kagi H, Kaneoka I, Lai Y, Prikhod'ko VS, Arai S. Fossil pressures of fluid inclusions in mantle xenoliths exhibiting rheology of mantle minerals: implications for the geobarometry of mantle minerals using micro-Raman spectroscopy. *Earth Planet Sci Lett*. 2002;198:511.
2. Yamamoto J, Otsuka K, Ohfuji H, Ishibashi H, Hirano N, Kagi H. Retentivity of CO_2 in fluid inclusions in mantle minerals. *Eur J Mineral*. 2011;23:805.
3. Arakawa M, Yamamoto J, Kagi H. Developing micro-raman mass spectrometry for measuring carbon isotopic composition of carbon dioxide. *Appl Spectrosc*. 2007;61:701.
4. Yokokura L, Hagiwara Y, Yamamoto J. Pressure dependence of micro-Raman mass spectrometry for carbon isotopic composition of carbon dioxide fluid. *J Raman Spectroscopy*. 2020;51:997.
5. Yamamoto J, Watanabe M, Nozaki Y, Sano Y. Helium and carbon isotopes in fluorites: implications for mantle carbon contribution in an ancient subduction zone. *J Vol Geotherm Res*. 2001;107:19.
6. Frezzotti ML, Ferrando S, Tecce F, Castelli D. Water content and nature of solutes in shallow-mantle fluids from fluid inclusions. *Earth Planet Sci Lett*. 2012;351-352:70.
7. Kawamoto T, Yoshikawa M, Kumagai Y, et al. Mantle wedge infiltrated with saline fluids from dehydration and decarbonation of subducting slab. *Proc Nat Acad Sci*. 2013;110:9663.
8. Andersen T, Burke EAJ, Neumann E-R. Nitrogen-rich fluid in the upper mantle: fluid inclusions in spinel dunite from Lanzarote, Canary Islands. *Contrib Mineral Petrol*. 1995;120:20.
9. Berkesi M, Káldos R, Park M, et al. Detection of small amounts of N_2 in CO_2-rich high-density fluid inclusions from mantle xenoliths *Eur J Mineral*. 2017;29:423.
10. Huraiova M, Dubessy J, Konecny P, *Plinius*. 1991;5:110.
11. Wang Y, Wang K, Konare Y, N_2-rich fluid in the vein-type Yangjingou scheelite deposit, Yanbian, NE China. *Sci Rep*. 2018;8:5662.
12. Yamamoto J, Takahata N, Sano Y, Yanagita M, Arai S, Prikhod'ko VS. Nitrogen and noble gas isotopic compositions of mantle xenoliths from Far Eastern Russia: implications for nitrogen isotopic characteristics of mantle wedge fluid. *Earth Planet Sci Lett*. 2020;534:116109.
13. Yokochi R, Marty B, Chazot G, Burnard P. Nitrogen in peridotite xenoliths: lithophile behavior and magmatic isotope fractionation. *Geochim Cosmochim Acta*. 2009;73:4843.
14. Capek T, Borysow J, Mazzoleni C, Moraldi M. Toward non-invasive measurement of atmospheric temperature using vibro-rotational Raman spectra of diatomic gases. *Remote Sensing*. 2020;12:4129.
15. Newton H, Walkup LL, Whiting N, et al. Comparative study of in situ N_2 rotational Raman spectroscopy methods for probing energy thermalisation processes during spin-exchange optical pumping. *Appl Phys B*. 2013;115:167.
16. Ohno H, Iizuka Y, Fujita S. Pure rotational Raman spectroscopy applied to N_2/O_2 analysis of air bubbles in polar firn. *J Glaciol*. 2021;67:903.
17. Bendtsen J. The rotational and rotation-vibrational Raman spectra of 14N2, 14N15N and 15N2. *J Raman Spectroscopy*. 1974;2:133.
18. Bendtsen J. High-resolution Fourier transform Raman spectra of the fundamental bands of14N15N and15N2. *J Raman Spectroscopy*. 2001;32:989.
19. Kim H, Aldén M, Brackmann C. Suppression of unpolarized background interferences for Raman spectroscopy under continuous operation. *Opt Express*. 2021;29:1048.
20. Knebl A, Domes R, Yan D, Popp J, Trumbore S, Frosch T. Fiber-enhanced Raman gas spectroscopy for 18 O-13 C-labeling experiments. *Anal Chem*. 2019;91:7562.
21. Wojdyr M. Fityk : a general-purpose peak fitting program. *J Appl Crystallogr*. 2010;43:1126.
22. Salter R, Chu J, Hippler M. Cavity-enhanced Raman spectroscopy with optical feedback cw diode lasers for gas phase analysis and spectroscopy. *Analyst*. 2012;137:4669.
23. Liu F, Yi F. Lidar-measured atmospheric N_2 vibrational-rotational Raman spectra and consequent temperature retrieval. *Opt Express*. 2014;22:27833.
24. Hagiwara Y, Takahata K, Torimoto J, Yamamoto J. CO_2 Raman thermometer improvement: comparing hot band and Stokes and anti-stokes Raman scattering thermometers. *J. Raman Spectroscopy*. 2018;49:1776.
25. Fukura S, Mizukami T, Odake S, Kagi H. Factors determining the stability, resolution, and precision of a conventional Raman spectrometer. *Appl Spectrosc*. 2006;60:946.
26. Hagiwara Y, Kawano T, Takahata K, Torimoto J, Yamamoto J, Raman J. *Spectroscopy*. 2021;52:1744.

How to cite this article: Yamamoto J, Hagiwara Y. Precision evaluation of nitrogen isotope ratios by Raman spectrometry. *Anal Sci Adv*. 2022;3:269–277.
https://doi.org/10.1002/ansa.202200020

Research Article
doi.org/10.1002/ansa.202200020
Chemistry Europe
European Chemical Societies Publishing

APPENDIX

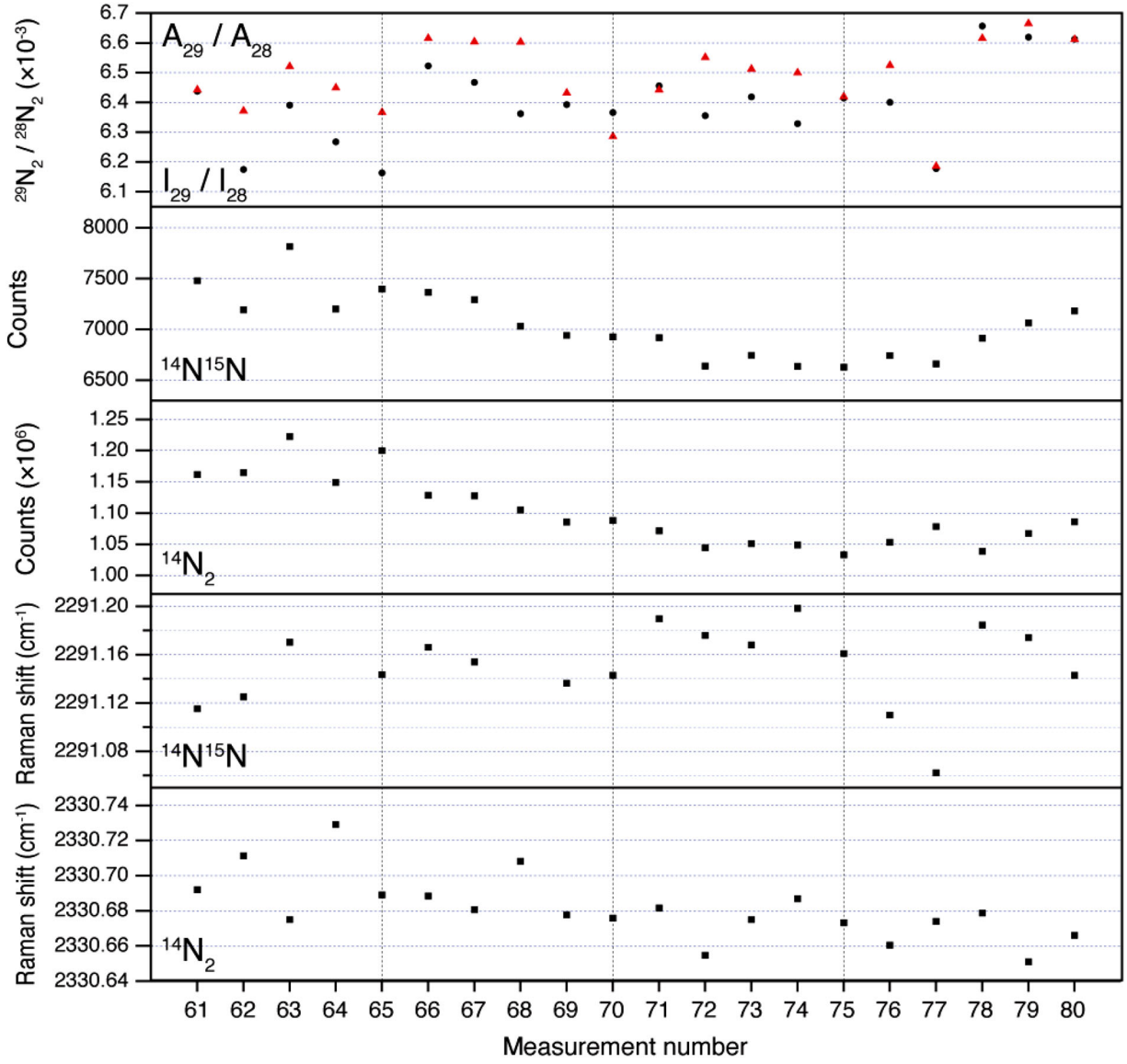

FIGURE A1 Fluctuation of peak height ratios, peak area ones, intensities, Raman shift of Raman peaks of 25 MPa N_2 fluid during measurement of data in 10^6-count region